Modeling, Design and Control of an Endoscope Manipulator for FESS

Weiyang Lin [a,b], David Navarro-Alarcon [a], Peng Li [b], Zerui Wang [a], Hiu Man Yip [a],
Yun-hui Liu [a,b], Michael C. F. Tong [a]

Abstract— This paper presents the development of an endoscope manipulator with passive and active structures for functional endoscopic sinus surgery (FESS). The 5-DoF passive structure has three translations and two rotations (T3R2) that allows the surgeon to manually place the endoscope near to the entry point during. The 4-DoF motorized structure (T2R2) actively controls the endoscope's position based on the surgeon's input commands. We analyze the reciprocal screw of the passive and active structures. The motion control system is based on a real-time Linux kernel that processes the commands from the surgeon and controls the manipulator's active joints. A user control interface based on an IMU fastened on the surgeon's foot is developed; this interface measures the foot's posture and through a series of gestures, it provides the desired pan/tilt/zoom motions of the camera. The developed endoscope manipulator allows the surgeon to conduct 'two-hand' operations while retaining direct control of the camera. We present an experimental study to validate the performance of the robotic prototype.

I. INTRODUCTION

Endoscopes are important imaging devices that are commonly used during minimally invasive surgical operations. These systems carry a camera and light source that capture in-body images, which are used by the surgeon to conduct the operation. During traditional functional endoscopic sinus surgery (FESS), the surgeon uses one hand to manipulate the endoscope and the other hand to manipulate the surgical instruments, see Fig. 1. This situation limits the surgeon's dexterity during the procedure, where in order to conduct two-hand operations, an assistant surgeon needs to manipulate the camera (this requires an excellent communication between both sides). Our aim in this paper, is to present a new foot-controlled robotic system that releases the hand-busy surgeon from the camera manipulation task, and enables him/her to retain direct control of its position.

Many robotic systems have been proposed in the literature to perform the endoscope manipulation task, see e.g. [1]. A cable driven surgical endoscope manipulator, with low cost and easy setup, is presented in [2]; in this work the surgeon controls the endoscope with voice commands, pedals, a joystick and head movements. There are some drawbacks with this approach, e.g. voice commands usually have a long delay time, joysticks do not allow to perform two-hand operations, foot pedals are not intuitive for multi-joint control, and head movements affects the surgeon's focus during surgery.

Fig. 1. In traditional FESS, the surgeon directly manipulates the endoscope.

In [3], a robotic prototype for trans-nasal neurosurgery is proposed. This endoscope manipulator provides the surgeon with real-time images, has a 2 rotational joints for pan and tilt motions, and a 2 translational joints for positioning the system. In [4], a computer-integrated surgical system using CAD/CAM models and data from surgical devices is proposed. The work [5] develops an remote center of motion (RCM) mechanism and two prototypes of endocavity ultrasound probe manipulators. In [6], an endoscope manipulator with eight motorized joints is proposed for sinus surgery; this robot is controlled using multiple foot pedals.

The endoscope manipulators mentioned above require a lot of time to set up the manipulator near the entry port. Note that these systems are controlled either by hands or multiple button-like pedals, rather than with the body's natural posture information. To contribute to this economically important problem, in this paper we present a new robotic system with the following key components: (i) a passive arm that can be used to manually position the endoscope near the entry port, (ii) an motorized endoscope manipulator which actively controls the camera motions in a decoupled manner, and (iii) an IMU-based control interface that commands the motion of the manipulator based on body postures.

The rest of the content is organized as follows: Section II presents the structure of manipulator, Section III analyzes the kinematics, Section IV describes the controller, Section V presents the experiments, and Section VI gives conclusions.

II. STRUCTURE OF THE MANIPULATOR

A. Design Specifications

The robot is designed to support and manipulate the endoscopic camera. For rapid positioning and accurate control purposes, the endoscope manipulator consists of a 5-DoF passive mechanism and a 4-DoF active mechanism, see Fig. 2. Note that to position the endoscope, we only need three
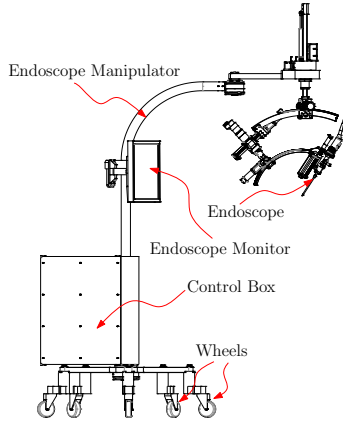
Fig. 2. Conceptual representation of the whole robotic system.

Fig. 3. Manipulator with passive and active parts.

translations and two rotations, therefore, the manipulator presented in this paper is clearly redundant.

The purpose of the robot is to help the surgeon to hold and manipulate the endoscope inside the nasal cavity. This endoscope is mounted on the manipulator's end-effector and provides the surgeon with real-time images that help him/her to conduct the operation. The passive mechanism allows the surgeon to manually position the endoscope near the entry port (i.e. the nostril) during the setup. The motorized mechanism receives the surgeon's commands and moves the endoscope to a specified position and orientation.

The control box of the robotic system (as shown in Fig. 2) includes the light source generator, camera receiver, embedded control board and DC motor drivers. The whole system can be manually moved with a wheeled platform, which can also be fixed by simply locking its wheels.

B. Passive Mechanism

The joint configuration of the passive positioning mechanism is $\mathcal{RRP}_g\mathcal{RR}$, where $\mathcal{R}$ and $\mathcal{P}$ denote a revolute joint and a prismatic joint, respectively (see Fig. 3). The passive mechanism is divided into two parts: $\mathcal{RRP}_g$ and $\mathcal{RR}$. The $\mathcal{RRP}_g$ mechanism has a SCARA-type structure that allows to position the active manipulator in 3D space. The controller, power source, motor drives and endoscope receiver are mounted on the control box, which rotates about the first revolute joint $\mathcal{R}$.

$\mathcal{P}_g$ denotes the prismatic joint of the gravity-balanced structure, which provides the linear 'up-and-down' translations, as shown in Fig. 3. The gravity-balanced structure is used to deal with load of the active manipulator, and hence simplify the manual positioning during the setup stage. This structure consists of an air-spring, spline axis, damper, and electromagnetic lock. The air-spring that we use is not a traditional constant force spring, it offers 70N force at its minimum compression and 90N force at its maximum compression; the structure nearly supports a payload of 80N. We incorporate a damper to keep balance for the non-constant air-spring; the damper's force is generated by a wedge-shaped piece of rubber which can be adjusted with a screw.
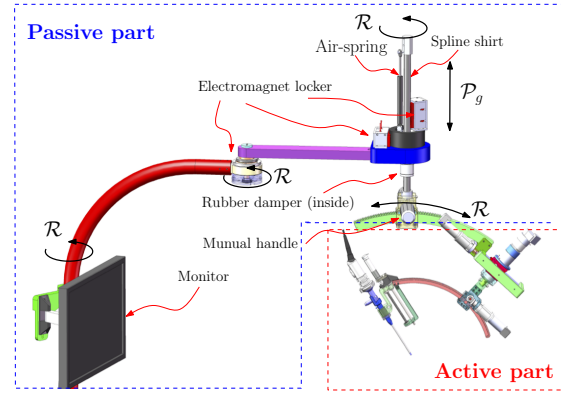
The last $\mathcal{RR}$ structure has an orthogonal rotary configuration whose axes intersect at the RCM point. This structure adopts a gear and an arc rack mechanism, with orthogonal transform matrices R_z and R_y. The gear and arc pairs have a high transmission ratio to simplify the joint design, and to make the RCM of $\mathcal{RR}$ outside the machine structure.

Traditional joint locking methods are typically electromagnetic clutches with power-off/on that locks/releases the joint (note that electromagnetic clutches usually do have not a compact structure).F or a lightweight and compact robot design, in our system we use a simple electromagnet that locks the passive orientation mechanism $\mathcal{RR}$ during the active endoscope manipulation. With the breaks released, the endoscope can be manually placed near the entry port of nasal cavity via the 5-DoF passive mechanism.

C. Active Manipulator

The active manipulator is conceptually depicted in Fig. 4. This part is composed of a linear joint $\mathcal{P}_l$, a universal joint $\mathcal{U}$ (for pan and tilt motions), and an insertion joint $\mathcal{P}_i$; its joint arrangement is $\mathcal{P}_l\mathcal{U}\mathcal{P}_i$ and its motion type is T2R2. The purpose of the active mechanism $\mathcal{P}_l\mathcal{U}\mathcal{P}_i$ is to help the surgeon to manipulate the endoscope via the control interface.

The RCM mechanism $\mathcal{U}\mathcal{P}_i$ of active manipulator $\mathcal{P}_l\mathcal{U}\mathcal{P}_i$ moves the endoscope in a spherical coordinate system, whose origin is located at the RCM point. The motion of the $\mathcal{U}\mathcal{P}_i$ structure can be described with spherical coordinates (r, θ, ϕ); this mechanism provides pivoting motion to the endoscope. The endoscopic camera captures the images of patient's nasal cavity with the full orientation capability of $\mathcal{U}\mathcal{P}_i$.

The linear joint $\mathcal{P}_l$ of the active manipulator translates the RCM point of the $\mathcal{U}\mathcal{P}_i$ mechanism along the direction of axis, as shown in Fig. 4. The direction of $\mathcal{P}_l$ needs to be manually tuned with the passive mechanism to make it parallel to the direction of the nasal cavity, so that surgeon can directly position RCM in the entry port by using the linear insertion joint. We remark that this motorized motion needs to be done only once at the beginning of the operation.
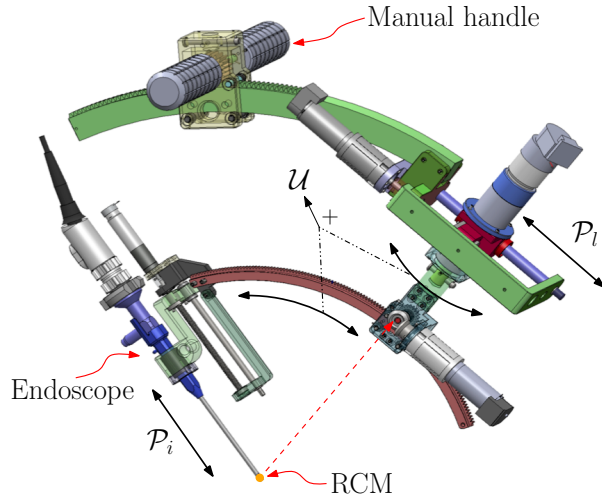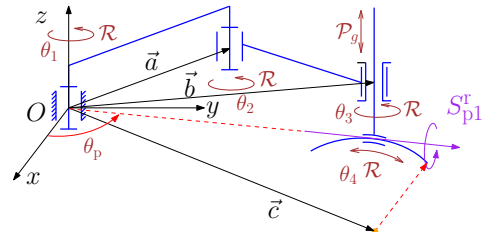
Fig. 4. Active manipulator.

Fig. 5. Motion analysis model of the passive mechanism.

Fig. 6. Motion analysis model of active manipulator.

III. MOTION TYPE ANALYSIS

The robotic manipulator is designed to actively control view of camera, therefore, precise positioning is not necessary. On the other hand, the location and orientation of patient's head on the operating table is difficult to be calibrated beforehand. Only by knowing in which directions the passive and active manipulator can be moved, the surgeon can (in principle) know how to operate the robotic system. For these reasons, the motion type of the passive and active mechanisms needs to be analyzed.

In order to obtain the mechanism's motion type, in this paper we use *screw theory* [7], which is a useful technique for analyzing the velocity and force vector spaces of system. The screw motion of the mechanism can show whether the motion type fulfils the task requirement. Let $S = [\vec{\omega}; \vec{v}]$ denote the screw vector, and $S^{\mathrm{r}} = [\vec{F}; \vec{M}]$ its reciprocal screw. The vectors $\vec{\omega}$ and $\vec{v}$ represent the rotational and linear velocities of the screw axis, respectively. For pure rotary motion, the linear velocity is $\vec{v} = (\vec{r} \times \vec{\omega})$, where $\vec{r}$ is the vector from the origin to the point on the rotational shaft. The vectors $\vec{F}$ and $\vec{M}$ denote the force and torque (moment) components of the reciprocal screw S^{r}. The symbol "$\circ$" denotes the reciprocal product operator [7], which pairs a screw with a reciprocal screw, and is defined as

$$S \circ S^{\mathrm{r}} = \vec{\omega} \cdot \vec{M} + \vec{v} \cdot \vec{F} \tag{1}$$

A schematic representation of the passive manipulator is shown in Fig. 5; $\vec{a}$, $\vec{b}$ and $\vec{c}$ denote vectors from the origin to the point on each rotational axis; θ_1, θ_2 and θ_3 are the angles of the first three rotational joints of $\mathcal{R}\mathcal{R}\mathcal{P}_g\mathcal{R}\mathcal{R}$; the final rotational angle of the arc rack component is $\theta_{\mathrm{p}} = \theta_1 + \theta_2 + \theta_3$.

Let $\vec{e}_{\mathrm{y}} = [0, 1, 0]^{\mathrm{T}}$ and $\vec{e}_{\mathrm{z}} = [0, 0, 1]^{\mathrm{T}}$ denote unit vectors, and $R_{\mathrm{z}}(\theta)$ denote the rotation matrix along the z axis with θ angle. The screw vectors $S_{\mathrm{p}1}$, $S_{\mathrm{p}2}$, $S_{\mathrm{p}3}$, $S_{\mathrm{p}4}$ and $S_{\mathrm{p}5}$ of the passive manipulator are

$$\begin{bmatrix} \vec{e}_{\mathrm{z}} \\ \vec{0} \end{bmatrix}, \begin{bmatrix} \vec{e}_{\mathrm{z}} \\ \vec{e}_{\mathrm{z}} \times \vec{a} \end{bmatrix}, \begin{bmatrix} \vec{e}_{\mathrm{z}} \\ \vec{e}_{\mathrm{z}} \times \vec{b} \end{bmatrix}, \begin{bmatrix} \vec{0} \\ \vec{e}_{\mathrm{z}} \end{bmatrix}, \begin{bmatrix} R_{\mathrm{z}}(\theta_{\mathrm{p}})\vec{e}_{\mathrm{y}} \\ \{R_{\mathrm{z}}(\theta_{\mathrm{p}})\vec{e}_{\mathrm{y}}\} \times \vec{c} \end{bmatrix} \tag{2}$$
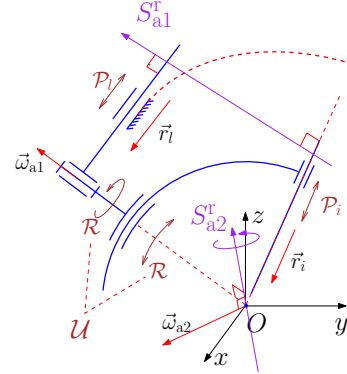
The reciprocal screw space is spanned by constraint force and torque vectors, the manipulator can only move in its orthogonal space (screw space). The screw space of passive mechanism is a 5-DoF linear space, so the dimension of the reciprocal screw space is 1. The reciprocal screw $S_{\mathrm{p}1}^{\mathrm{r}}$ can be calculated by the reciprocal product with (2) according to

$$S_{\mathrm{p}i} \circ S_{\mathrm{p}1}^{\mathrm{r}} = 0, \quad i = 1, \cdots, 5 \tag{3}$$

The obtained reciprocal screw is as follows:

$$S_{\mathrm{p}1}^{\mathrm{r}} = \begin{bmatrix} \vec{0} & \vec{M}_{\mathrm{p}} \end{bmatrix}^{\mathrm{T}} \tag{4}$$

Eq. (4) is important in our analysis because it shows that the passive mechanism cannot rotate in the direction given by $\vec{M}_{\mathrm{p}} = \vec{e}_{\mathrm{z}} \times (R_{\mathrm{z}}(\theta_{\mathrm{p}})\vec{e}_{\mathrm{y}}) = [\cos\theta_{\mathrm{p}}, \sin\theta_{\mathrm{p}}, 0]^{\mathrm{T}}$, see Fig. 5. The analysis shows that the passive manipulator has a T3R2 motion type, and that the constraint motion is a rotation around the $\vec{M}_{\mathrm{p}}$ direction. Therefore, in order to manipulate the endoscope with all directions, the active part needs to provide the constraint motion.

The motion analysis of the active manipulator is conceptually depicted in Fig. 6. Let the origin point of the coordinate system be the RCM of manipulator; the screw vectors $S_{\mathrm{a}1}, S_{\mathrm{a}3}, S_{\mathrm{a}3}, S_{\mathrm{a}4}$ of the active part can be written as

$$\begin{bmatrix} \vec{0} \\ \vec{r}_l \end{bmatrix}, \begin{bmatrix} \vec{\omega}_{\mathrm{a}1} \\ \vec{0} \end{bmatrix}, \begin{bmatrix} \vec{\omega}_{\mathrm{a}2} \\ \vec{0} \end{bmatrix}, \begin{bmatrix} \vec{0} \\ \vec{r}_i \end{bmatrix} \tag{5}$$

Let the vector $\vec{F}_{\mathrm{a}} = (\vec{r}_l \times \vec{r}_i)/\|\vec{r}_l \times \vec{r}_i\|$ denote the orthogonal complement of $\vec{r}_l$ and $\vec{r}_i$, and let $\vec{M}_{\mathrm{a}} = (\vec{\omega}_{\mathrm{a}1} \times \vec{\omega}_{\mathrm{a}2})/\|\vec{\omega}_{\mathrm{a}1} \times \vec{\omega}_{\mathrm{a}2}\|$ denote the orthogonal complement of $\vec{\omega}_{\mathrm{a}1}$ and $\vec{\omega}_{\mathrm{a}2}$. Similar to the passive manipulator, the relationship between the reciprocal screw and the screw vector is

$$S_{\mathrm{a}i} \circ S_{\mathrm{a}j}^{\mathrm{r}} = 0, \quad i = 1, \cdots, 4 \text{ and } j = 1, 2 \tag{6}$$

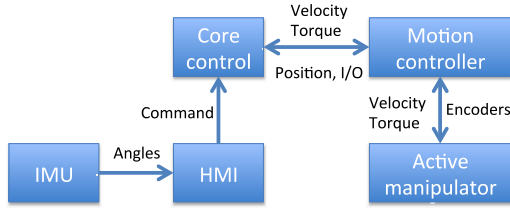Fig. 7.   Framework of the control system.

Fig. 8.   The IMU-based control interface.

The reciprocal screw is calculated as follows:

$$S_{a1}^r = \begin{bmatrix} \vec{F}_a \\ \vec{0} \end{bmatrix}, \ S_{a2}^r = \begin{bmatrix} \vec{0} \\ \vec{M}_a \end{bmatrix} \tag{7}$$

Eq. (7) shows that the active manipulator has a T2R2 motion type; this mechanism is constrained by the reciprocal screw and cannot move in the $\vec{F}_a$ direction and cannot rotate in $\vec{M}_a$ direction.

IV. MOTION CONTROLLER

A. Control System Architecture

The control system is composed of a Linux-based industrial PC, an embedded Galil DMC-1440 control board with analog outputs, Maxon current amplifiers, electromagnets, wireless communication modules and an IMU. The Galil control board decodes the motor's position and outputs the analog control signal (calculated by an inner PID algorithm) to the current amplifiers. One linear joint and two rotary joints of the active manipulator are controlled in velocity mode. For safety reasons, the motor of the insertion joint is controlled in current mode; this joint moves with a small and constant feed-forward force, which can help to prevent applying excessive forces to the tissues. A schematic representation of the control system is shown in Fig. 7.

For safety purposes, the control system of the surgical robots must operate with a deterministic hard real-time behavior, that is, all the sensor's signals and motion control algorithms must operate with strict sample time. We developed a Linux-based real-time motion control system, which uses the Xenomai kernel patch to achieve a hard real-time performance. The control system processes all the sensor feedback, computes kinematic algorithms, and handles the command and event errors. The control software is divided into two parts: robot control core and human machine interface (HMI). The robot control core manages the hardware resources and is in charge of implementing the low-level control tasks, such as computing the motor's velocity and current commands, enabling and disabling the algorithms, communicating with the HMI and monitoring the error events.

B. IMU Control Interface

In our robotic FESS, the surgeon must directly manipulate the tools with his/her hands, therefore, a joystick interface cannot be used to operate the system. A simple solution to this could be to place foot pedals under the operating table. For this kind of devices, each button is similar to a '1-bit'

information generator, therefore, it requires many buttons to control multiple joints; to add more buttons, makes it difficult for the surgeon to operate robot.

Using body's posture informations to control the endoscope seems a feasible solution, since the body's posture contains many DoFs. In our system we use an IMU to control the active manipulator, see Fig. 8. An IMU with an Arduino micro-controller unit is fastened to the surgeon's foot to measure the foot's orientation; the measured feedback is sent to PC via bluetooth channel. The HMI receives the feedback data, identifies the foot gesture from user, and sends the motion command to the core control application.

The IMU interface measures the pitch, yaw and roll angles (α, β, γ) of the foot; it communicates with the control system via 57600 bps bluetooth. We use these feedback angles to implement the following actions: (1) enable/disable the whole control process, (2) select the active joint, and (3) command the joint's forward/backward motion. The foot posture commands are shown in Fig. 9 and Fig. 10. The interface control logic is described with following set of rules:

> **if** $\alpha < 60° \rightarrow \alpha \geq 60° \rightarrow \alpha < 60° \rightarrow \alpha \geq 60°$ **then**
>   "Enable/disable control process"
> **end if**
> **if** $\alpha < 10°$ and $(\gamma < 15° \ \rightarrow \ \gamma \geq 15°)$ **then**
>   "Change to previous active joint"
> **else if** $\alpha < 10°$ and $(\gamma > -15° \ \rightarrow \ \gamma \leq -15°)$ **then**
>   "Change to next active joint"
> **end if**
> **if** $10° \leq \alpha < 60°$ and $\beta \leq -12°$ **then**
>   "Move the active joint backwards"
> **else if** $10° \leq \alpha < 60°$ and $\beta \geq 12°$ **then**
>   "Move the active joint forwards"
> **end if**

We use the symbol $A \rightarrow B$ to represent the change from state A to B. In our application, we calibrate the threshold for α, β and γ depending on the user. We use the pitch angle α that is shown in Fig. 9 to enable/disable the control process.

Fig. 10 shows the foot gestures used to control the motor and to select the active joint (i.e. the one being controlled). For safety reasons and to simplify the operation, our system can only control the motion of one joint at the time.

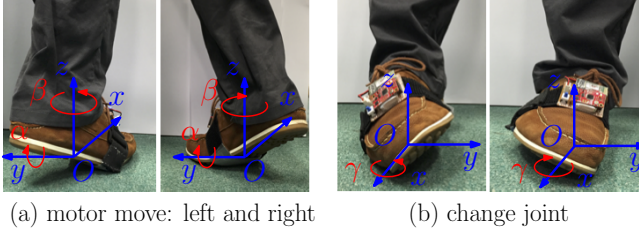Fig. 9. Pitch angle is used for enable and disable.

(a) motor move: left and right   (b) change joint

Fig. 10. Motor move command and change active joint.

V. ROBOT PROTOTYPE AND EXPERIMENTS

A. Robot Prototype

The developed prototype of the endoscope manipulator is shown in Fig. 11. This manipulator adopted two arc racks to avoid any machine components from colliding with the patient's head. At the beginning of the operation, the surgeon uses a handle to manually place the endoscope near the nasal cavity. The image feedback provided by camera is then used by the surgeon to guide the active insertion of the endoscope inside the cavity.

The active manipulator is shown in Fig. 12. This mechanism is driven by four DC motors, which can be directly controlled by surgeon through the IMU device.

To conduct the surgical operation, the active part of the system is the most important one, since these motorized joints directly control the orientation of captured images. Fig. 13 illustrates endoscope positioning experiments with a human head model. This figure depicts the maximum range of motions that the manipulator can achieve when inserted into the nasal cavity. Note that the range showed in the figures for the pan and tilt joints is smaller than the one the robot can actually achieve. However, in order to avoid any injuries to the patient, the system is restricted to smaller rotational motions.

B. Ex-vivo Experiment

To validate the performance of the robotic prototype, we conducted an ex-vivo experimental study with five cadaver heads, at the Prince of Wales Hospital in Hong Kong. As Fig. 14 shows, the developed robotic manipulator provides the surgeon with a hand-free method to position the camera. This approach allows surgeons to use both hands to manipulate the instruments according to the captured images. In these experiments, it took less than two minutes for one surgeon to setup the manipulator and place the endoscope inside the nasal cavity.
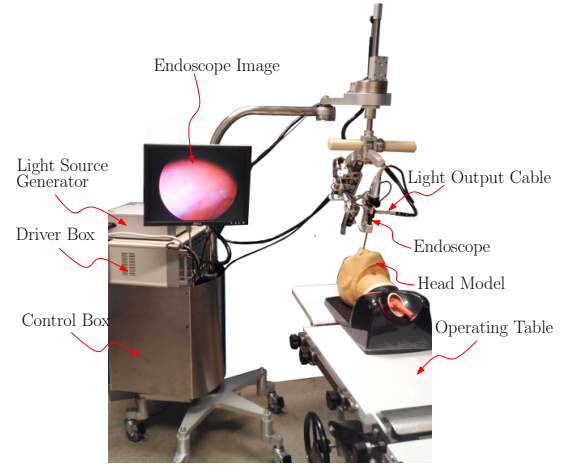

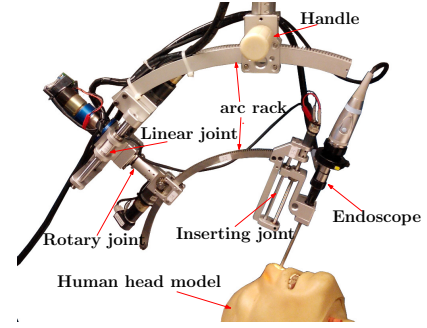Fig. 11. Prototype of robotic assistant.

Fig. 12. Active part of endoscope manipulator.

Fig. 15 shows the IMU and joint angles measured during the experiment. This figure shows how the surgeon enables the control process, then switches the active joint, and finally commands its desired motion.

We also conducted a force testing study to determine the applied force that breaks/damages the soft tissues inside the nasal cavity; we used the force measuring device shown in Fig. 16. For this experiment, the surgeon manually pushed with the device the tissues. The measured force for this experiment is shown in Fig. 17, where we can see that the tissue of the specimen breaks around 25N. To guarantee the safe operation of the robot, the maximum current of the insertion joint needs to be set such that the applied force of the tip do not exceed 10N.
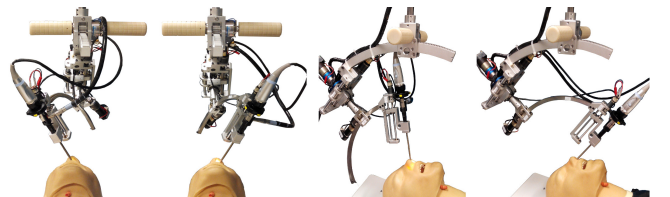

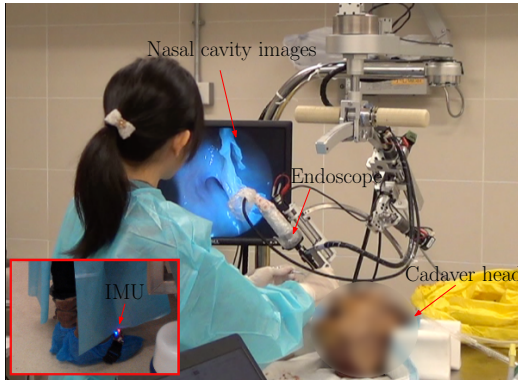Fig. 13. The limit position of pan and tilt angles

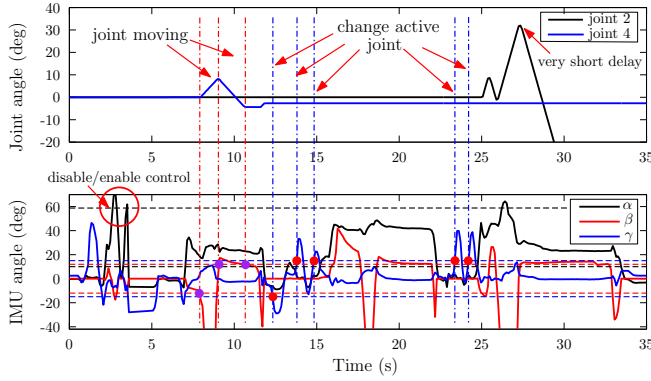Fig. 14. Ex-vivo experiments with the robotic prototype for FESS.

Fig. 16. Ex-vivo force testing experiment.

Fig. 15. IMU and joint's data of the experiment
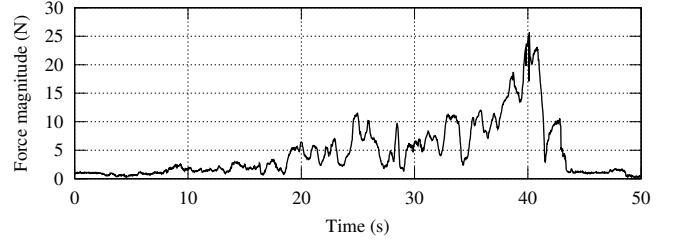
Fig. 17. Force magnitude of the tissue breaking experiment.

VI. CONCLUSIONS

In this paper, we developed a new surgical endoscope manipulator to assist the surgeon during a FESS. The system is composed of a 5-DoF passive positioning arm, and a 4-DoF active robotic manipulator. To control its motion, we proposed an IMU-based human-robot interface which is attached to the surgeon foot; the ex-vivo experiments showed that this interface is intuitive and easy to use.

As future work, we would like to incorporate automatic control mode into the system, e.g. the use of image-based method to automatically position the endoscopic camera inside the nasal cavity. To improve the safety of the system, we would like to integrate the feedback of a force/moment sensor into our control methods.

ACKNOWLEDGEMENTS

REFERENCES

[1] C.H. Kou, J. S. Dai, P. Dasgupta. "Kinematic design considerations for minimally invasive surgical robots: an overview," *Int. J. Med. Robot. Comp.*, Vol. 8, pp. 127-145, Jun. 2012.

[2] P. Berkelman, P. Cinquin, J. Troccaz, et al. "A compact, compliant laparoscopic endoscope manipulator," in *Proc. IEEE Int. Conf. Robotics and Automation*, 2002, pp. 1870–1875.
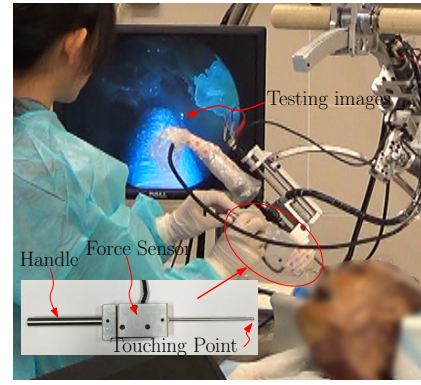
[3] Y. Koseki, T. Washio, K. Chinzei, et al. "Endoscope manipulator for trans-nasal neurosurgery, optimized for and compatible to vertical field open MRI," in *Proc. Int. Conf. Medical Image Computing and Computer-Assisted Intervention*, 2002, pp. 114–121.

[4] R. H. Taylor, D. Stoianovici. "Medical robotics in computer-integrated surgery," in *IEEE Trans. Robot. Automat.*, vol. 19, pp. 765–781, Oct. 2003.

[5] D. Stoianovici, C. Kim, F. Schäfer, et al. "Endocavity ultrasound probe manipulators", in *IEEE/ASME Trans. Mechatronics*, vol. 18, pp. 914–921, Jan. 2013.

[6] P. Li, H. M. Yip, D. Navarro-Alarcon, Y. H. Liu, M. Tong, and I. Leung, "Development of a robotic endoscope holder for nasal surgery," in *Proc. Int. Conf. Information and Automation*, 2013, pp. 1194–1199.

[7] J. K. Davidson, K. H. Hunt, et al. "Robots and Screw Theory: Applications of Kinematics and Statics to Robotics," OXFORD, 2004.

[8] C. Last, S. Winkelbach, F. M. Wahl, et al. "A model-based approach to the segmentation of nasal cavity and paranasal sinus boundaries," in *Proc. DAGM Conf. Pattern Recognition* 2010, pp. 333–342.

[9] S. W. Kang, C. S. Park, J. J. Jeong, et al. "Robot-assisted endoscopic surgery for thyroid cancer: experience with the first 100 patients," *J. Surg. Endosc.*, vol. 23, pp. 2399–2406, Nov. 2009.

[10] C. Vara-Thorbeck, V. F. Munoz, R. Toscano, et al. "A new robotic endoscope manipulator," *J. Surg. Endosc.*, vol. 15, pp. 924–927, Sep. 2001.

[11] B. Mitchell, J. Koo, I. Iordachita, et al. "Development and Application of a New Steady-Hand Manipulator for Retinal Surgery," in *Proc. IEEE Int. Conf. Robotics and Automation*, 2007, pp. 623–629.

[12] K. Taniguchi, A. Nishikawa, M. Sekimoto. "COVER: compact oblique-viewing endoscope robot for laparoscopic surgery," *Int. J. Comput. Assist. Radiol. Surg.*, pp. 207–209, Feb. 2006.